

---

# WESTWORLD: A KNOWLEDGE-ENCODED SCALABLE TRAJECTORY WORLD MODEL FOR DIVERSE ROBOTIC SYSTEMS

---

**Yuchen Wang\***  
Department of Computer Science  
William & Mary  
ywang142@wm.edu

**Jiangtao Kong\***  
Department of Computer Science  
William & Mary  
jkong01@email.wm.edu

**Sizhe Wei**  
School of Aerospace Engineering  
Georgia Institute of Technology  
swei@gatech.edu

**Xiaochang Li**  
Department of Computer Science  
William & Mary  
xli59@wm.edu

**Haohong Lin**  
College of Engineering  
Carnegie Mellon University  
haohong1@andrew.cmu.edu

**Hongjue Zhao**  
Department of Computer Science  
University of Illinois Urbana-Champaign  
hongjue2@illinois.edu

**Tianyi Zhou**  
Department of Computer Science  
Mohamed bin Zayed University of Artificial Intelligence  
tianyi.zhou@mbzuai.ac.ae

**Lu Gan**  
School of Aerospace Engineering  
Georgia Institute of Technology  
lgan@gatech.edu

**Huajie Shao<sup>†</sup>**  
Department of Computer Science  
William & Mary  
hshao@wm.edu

## ABSTRACT

Trajectory world models play a crucial role in robotic dynamics learning, planning, and control. While recent works have explored trajectory world models for diverse robotic systems, they struggle to scale to a large number of distinct system dynamics and overlook domain knowledge of physical structures. To address these limitations, we introduce *WestWorld*, a **know**ledge-**EN**coded **SC**alable **TR**ajectory **WO**rd model for diverse robotic systems. To tackle the scalability challenge, we propose a novel system-aware Mixture-of-Experts (Sys-MoE) that dynamically combines and routes specialized experts for different robotic systems via a learnable system embedding. To further enhance zero-shot generalization, we incorporate domain knowledge of robot physical structures by introducing a structural embedding that aligns trajectory representations with morphological information. After pretraining on 89 complex environments spanning diverse morphologies across both simulation and real-world settings, *WestWorld* achieves significant improvements over competitive baselines in zero- and few-shot trajectory prediction. Additionally, it shows strong scalability across a wide range of robotic environments and significantly improves performance on downstream model-based control for different robots. Finally, we deploy our model on a real-world Unitree Go1, where it demonstrates stable locomotion performance (see our demo on the website). The code will be available upon publication.

## 1 Introduction

Trajectory world models [17, 39, 46] are essential for robotic dynamics learning [44], planning, and control based on *low-level sensory data*. However, building a trajectory world model for diverse robotic systems poses two key

---

\*These authors contributed equally to this work.

<sup>†</sup>Corresponding author.

challenges: *i) sensor and actuator heterogeneity*, where the variance in types and sampling rates hinders shared representations, and *ii) system dynamics gaps* caused by diverse kinematic structures across different robotic systems.

To address these challenges, a few recent studies [33, 46] discretize continuous states and actions across diverse systems into tokens via quantization and leverage flexible Transformer architectures for joint training. Although these approaches enable multi-system pretraining within a single dense model, they still face *scalability and generalization limitations* across diverse robotic dynamics for two main reasons. *First*, existing approaches force different system dynamics to share a common set of model parameters, leading to gradient conflicts and negative transfer that impede effective scaling as robot diversity grows. *Second*, these methods overlook robot morphological information when modeling trajectories, thereby lacking the physical inductive biases required for zero-shot generalization to unseen robotic systems.

To overcome these limitations, we develop *WestWorld*, a knowledge-encoded scalable trajectory world model that incorporates domain knowledge of robot morphology to learn the underlying dynamics of diverse robotic systems (see Fig. 1). Developing such a model poses two *key challenges*: *i) learning distinct system dynamics at scale* while avoiding task interference across different robots, and *ii) incorporating physical structural information as an inductive bias to enhance zero-shot generalization*. To address the first challenge of scalability, we propose a system-aware mixture-of-experts (Sys-MoE) that implicitly learns distinct system dynamics through expert learning. Unlike existing trajectory world models, which learn multiple system dynamics using a single large dense model, the proposed Sys-MoE dynamically combines and routes specialized experts for different robotic systems via a learnable system embedding. This design mitigates task interference across robots, thus significantly improving scalability. For the second challenge of generalization, we introduce a structure-based channel embedding that aligns low-level state trajectories with morphology information, thereby improving the model’s ability to generalize to unseen robotic systems.

We pretrain the proposed *WestWorld* on 89 complex environments using a combination of simulated and real-world data. Extensive experiments show that our method substantially outperforms strong baselines in both zero-shot and few-shot trajectory prediction. Moreover, it enables scalable training across diverse robotic systems without sacrificing performance and significantly improves the performance of downstream tasks such as model-based control.

**Our contributions include:** 1) We propose *WestWorld*, a novel system-aware MoE architecture for scaling up the training of trajectory world models across diverse robotic systems; 2) We introduce knowledge-encoded structural embedding that provides an explicit inductive bias to enhance zero- and few-shot generalization to unseen robotic systems; 3) We conduct extensive experiments to verify the scalability and generalizability of our method, showing its superiority over strong baselines; and 4) We apply our model to downstream model-based control and further extend it to real-world Unitree Go1 deployment, demonstrating its strong performance in planning tasks.

## 2 Related Work

**World Models for Single Robots.** World models [17] serve as a foundational tool for sequential decision-making in embodied agents [40, 26], enabling them to model, understand, and predict environmental dynamics. In robotics, one line of work [2, 7] leverages video generation models as world models to synthesize temporally coherent observations, thereby implicitly capturing underlying physical dynamics. Another line of research develops action-conditioned *dynamics* world models that explicitly predict future states for planning and control [14, 9, 48, 19, 8]. These dynamics world models can be broadly categorized into video world models and trajectory world models, offering complementary perspectives for learning physical dynamics.

In this work, we focus on *studying low-level trajectory world models*. Generalizing such models across diverse robotic systems is non-trivial, since trajectories are derived from heterogeneous sensors and actuators with mismatched channel semantics across systems. Thus, most existing trajectory world models [43, 19, 8] are tailored to a single robot, and transferring to new platforms typically requires retraining or substantial adaptation. In contrast, our work aims to learn a unified trajectory world model that scales across diverse robotic systems.

**Trajectory World Model for Diverse Robotics.** Recent works [18, 46, 33] have explored trajectory world models for diverse robotic systems. A key challenge is handling varying sensor and actuator dimensionalities across different robots. A common strategy is to zero-pad inputs to a shared maximum dimension [18]. However, padding-based approaches suffer from dimensionality limits and often degrade generalization across environments [46]. To address this, a few recent studies [33, 46] treat states and actions as token sequences and jointly train flexible Transformer architectures across multiple robots. Despite enabling joint pretraining across diverse robots, their scalability and generalization remain limited. First, most existing methods learn heterogeneous robotic systems using a single shared set of model parameters, which induces cross-system interference as robot diversity grows and makes scaling difficult.

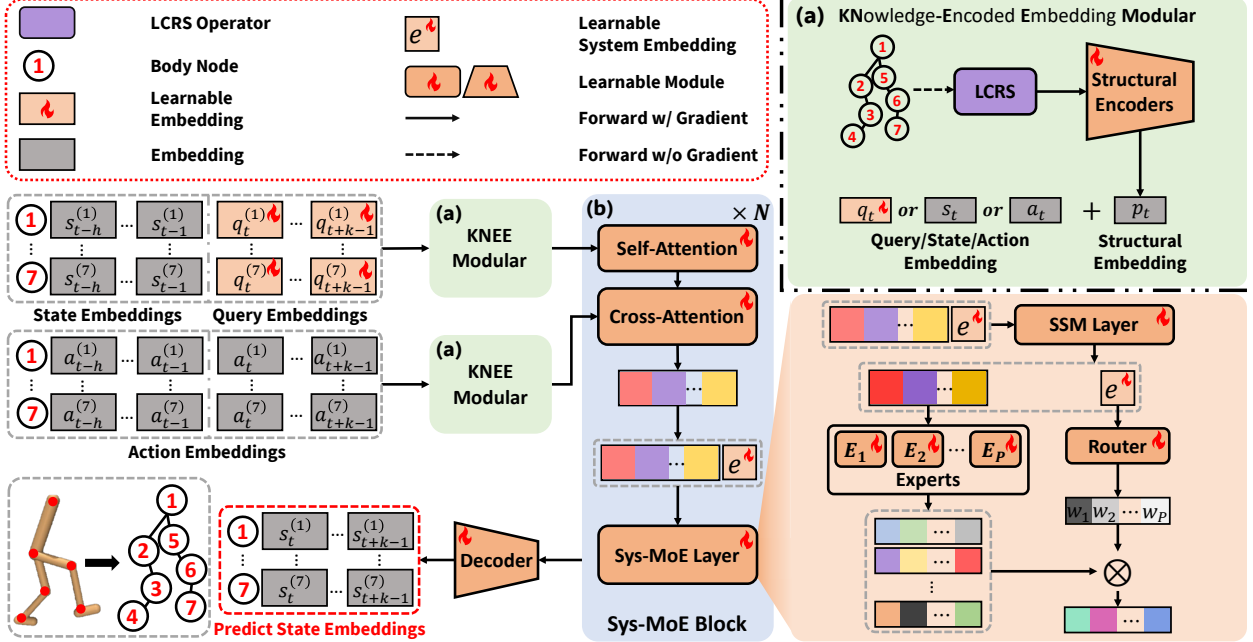


Figure 1: The overall architecture of our proposed WestWorld, consisting of two core components: (a) a Knowledge-Encoded Embedding Modular that injects structural embeddings as an inductive bias into trajectory representations, and (b) a System-aware MoE block that models diverse system dynamics via system-aware expert routing.

Second, these methods treat trajectories purely as token sequences while ignoring robot morphology information, which results in poor zero-shot generalization to unseen robotics.

Unlike prior works, we propose a system-aware MoE model that incorporates robot structural information to enable both scalable pretraining and strong zero-shot performance.

### 3 Preliminaries

**Notations.** The detailed descriptions of important notations are presented in Table 5 in Appendix A.

**Problem Statement.** A robotic system can be viewed as a controlled dynamical process with state space  $\mathcal{S}$ , action space  $\mathcal{A}$ , and transition dynamics  $f$ . In practice, the state  $s_t \in \mathcal{S}$  consists of physical sensor readings such as joint positions and joint velocities, while the action  $a_t \in \mathcal{A}$  represents control commands such as joint torques.

Model-based control relies on an internal dynamics model to support planning by rolling out candidate action sequences in imagination [26].

In this work, we use a *trajectory world model* purely as a dynamics model [35, 26, 16] that predicts future states  $s$  conditioned on action interactions  $a$ . Formally, a world model parameterizes a transition distribution

$$p_{\theta}(s_{t+1} | s_{1:t}, a_{1:t}), \quad s_t \in \mathcal{S}, a_t \in \mathcal{A}, \quad (1)$$

which can be used to unroll state trajectories under a proposed action sequence. A rollout induces a trajectory

$$\tau = (s_0, a_0, s_1, a_1, \dots, s_t, a_t), \quad (2)$$

and the model is trained on the recorded trajectories  $\mathcal{D} = \{\tau_i\}$  by maximizing predictive accuracy of future states.

*The goal of this work* is to develop a pretrained trajectory world model to learn the system dynamics across varying robotic systems and environments. Given a trajectory dataset from  $n$  distinct robotic systems,  $\{\mathcal{D}_1, \mathcal{D}_2, \dots, \mathcal{D}_n\}$ , our objective is to learn a single model  $\theta$  that captures the dynamics of all  $n$  systems. Specifically, given a history of  $h$  past states and actions, the model tries to predict the next  $k$  future states, conditioned on a sequence of  $k$  future actions.

## 4 Proposed Method

### 4.1 Overview of WestWorld

To enable scalable pretraining and zero-shot generalization across diverse robotic systems, we propose WestWorld, a knowledge-encoded scalable trajectory world model with a system-aware Mixture-of-Experts (MoE) design. As shown

in Fig. 1, the proposed model consists of two core components: (1) *Knowledge-Encoded Embedding Modular* and (2) *System-Aware MoE*.

The *core idea* is to first perform channel-wise normalization and discretize each scalar variable for tokenization. The resulting representations are then processed by *Knowledge-Encoded Embedding Modular*, which extracts the robot’s morphological connectivity and injects structural embeddings as an inductive bias into trajectory representations. These structure-aware embeddings are subsequently fed into multiple *System-Aware MoE* blocks for dynamics modeling. Finally, a linear decoder maps the hidden states to future trajectory predictions. We detail these two core components in the following.

## 4.2 Knowledge-Encoded Embedding Modular

**Motivation.** Existing trajectory world models are predominantly data-driven, relying solely on state-action observations and largely ignoring domain knowledge that different robotic morphologies should obey distinct physical constraints. The lack of encoding explicit structural information makes it difficult for these models to capture the underlying system dynamics and limits their ability to generalize across environments. We hypothesize that robots with similar connectivity patterns often exhibit shared high-level dynamical behaviors (e.g., SLIP-like locomotion [34]). This insight motivates us to incorporate morphological connectivity into model design as an inductive bias. Below, we first introduce the trajectory data tokenization before diving into proposed knowledge-encoded structural embedding.

**Trajectory Tokenization.** Given a trajectory, we treat each state or action dimension at time step  $t$  as a *scalar channel*. Let  $x_t^{(m)} \in \mathbb{R}$  denote the value of channel  $m$  at time  $t$ , where  $m$  represents the index of state channels or action channels. We apply channel-wise min-max normalization, and discretize it into a  $K$ -bin categorical vector through  $\phi: \mathbb{R} \rightarrow \mathbb{R}^K$  following [46]. We then map  $\phi(x_t^{(m)})$  to a  $d$ -dimensional embedding via a learned projection. After that, we incorporate timestep embeddings, channel order index embeddings, and modality indicator (state or action) embeddings, yielding  $z_t^{(m)} \in \mathbb{R}^d$ . For convenience, we stack the per-channel embeddings from states and actions at time step  $t$  into  $\mathbf{S}_t \triangleq [\mathbf{s}_t^{(1)}; \dots; \mathbf{s}_t^{(M_s)}]^\top \in \mathbb{R}^{M_s \times d}$  and  $\mathbf{A}_t \triangleq [\mathbf{a}_t^{(1)}; \dots; \mathbf{a}_t^{(M_a)}]^\top \in \mathbb{R}^{M_a \times d}$ , where  $M_s$  and  $M_a$  are the numbers of state and action channels.

**Knowledge-Encoded Structural Embedding.** To incorporate morphology structure priors into latent representations, we introduce a knowledge-encoded structural embedding, as shown in Fig. 1 (a). Specifically, we first model each articulated object as a rooted kinematic tree and convert it to a binary tree using the left-child-right-sibling (LCRS) transformation [22]. Each body node is assigned three traversal indices from pre-/in-/post-order walks. For object  $i$  and its body node  $j$ , let  $(\pi_{\text{pre}}^{i,j}, \pi_{\text{in}}^{i,j}, \pi_{\text{post}}^{i,j})$  denote these indices. In scenes with multiple articulated objects, we additionally assign an object identifier  $\pi_{\text{obj}}^i$ : the robot is indexed as  $\pi_{\text{obj}}^i = 0$ , and other objects are ordered by increasing Euclidean distance to the robot (see Appendix B for an example). With this tuple indices, we can uniquely identify each robot body node in the LCRS-converted binary tree derived from the robot’s structure. Then, we embed these indices to obtain a structure embedding:

$$\mathbf{p}^{(i,j)} = \text{Concat}\left(e_{\text{obj}}(\pi_{\text{obj}}^i), e_{\text{pre}}(\pi_{\text{pre}}^{i,j}), e_{\text{in}}(\pi_{\text{in}}^{i,j}), e_{\text{post}}(\pi_{\text{post}}^{i,j})\right). \quad (3)$$

where each  $e_{\{\text{obj}, \text{pre}, \text{in}, \text{post}\}}(\cdot)$  denotes a structural encoder that maps a discrete index to a  $d/4$ -dimensional vector, and their concatenation forms  $\mathbf{p}^{(i,j)} \in \mathbb{R}^d$ . Finally, we inject morphology knowledge by adding  $\mathbf{p}^{(i,j)}$  to the corresponding state/action embeddings, yielding structure-aware trajectory embeddings that are used as inputs to our model.

## 4.3 System-Aware MoE Block

**Motivation.** Robotic systems with diverse morphologies often exhibit markedly different dynamics, making it difficult to develop a single unified model that accurately captures their underlying dynamics. When such dissimilar dynamics are trained simultaneously using shared parameters, optimization is prone to gradient conflicts and task interference, leading to poor scalability. To address this challenge, we introduce a novel system-aware Mixture-of-Experts (Sys-MoE) block for learning distinct system dynamics, in which each expert specializes in a basis dynamics module. Our *key insight* is that complex system dynamics can be effectively approximated by composing a set of basis dynamics with system-dependent coefficients.

**Block design.** To scale joint training across diverse robotic systems while mitigating interference, we parameterize the transition model in Eq. (1) with a stack of *Sys-MoE Blocks*. Each block contains two parts: *i*) an attention-based aggregation module that fuses state-action information, and *ii*) a system-aware MoE layer that captures diverse system dynamics. We detail the two parts below.

**i) Attention-based aggregation.** As shown in Fig. 1(b), we use attention to aggregate information across state channels and to inject action-dependent control signals, while naturally supporting variable state/action dimensionalities across systems. Concretely, we apply: 1) self-attention to capture correlations among state variables, and then use 2) cross-attention to condition state features on the action embeddings. To enable  $k$ -step prediction in a single forward pass, we concatenate the history state embeddings with  $k$  learnable query embeddings  $\{\mathbf{q}_t, \dots, \mathbf{q}_{t+k-1}\}$ , which serve as latent queries for future states.

At each time step, self-attention is computed as

$$\tilde{\mathbf{S}}_t = \text{LN}\left(\mathbf{S}_t + \text{Self-Atten}(\mathbf{S}_t)\right), \quad (4)$$

where self-attention is applied along the state channel, and  $\text{LN}(\cdot)$  is layer normalization. We then condition  $\tilde{\mathbf{S}}_t$  on the action embeddings  $\mathbf{A}_t$  via multi-head cross-attention:

$$\hat{\mathbf{S}}_t = \text{LN}\left(\tilde{\mathbf{S}}_t + \text{Cross-Atten}(\tilde{\mathbf{S}}_t, \mathbf{A}_t)\right), \quad (5)$$

This operation injects action-dependent signals while remaining compatible with variable action dimensionalities.

**ii) System-aware MoE layer.** After obtaining the action-conditioned latent states above, we model continuous-time system dynamics using a system-aware Mixture-of-Experts (Sys-MoE) layer, as shown in Fig. 1(b). Unlike the MoE design commonly used in large language models, where routing selects experts to directly produce token embeddings from the input, our routing is *system-aware*. Specifically, we introduce a learnable system embedding that propagates through the SSM to extract system-level properties of the underlying dynamics. The resulting system embeddings are then used to compute mixture weights over experts, so that the model forms a system-conditioned combination of different experts.

Let  $L = h + k$  be the number of state embeddings after concatenating history states with  $k$  queries. For each state channel  $m$ , we denote the attention outputs as  $\hat{\mathbf{S}}_{1:L}^{(m)} = \{\hat{\mathbf{s}}_{t-h:t-1}^{(m)}, \hat{\mathbf{s}}_{t:t+k-1}^{(m)}\}$ , where the last  $k$  tokens correspond to the query positions. We append a learnable system embedding  $\mathbf{e} \in \mathbb{R}^d$  to attention outputs, yielding

$$\bar{\mathbf{S}}^{(m)} = \text{Concat}\left(\hat{\mathbf{S}}_{1:L}^{(m)}, \mathbf{e}\right). \quad (6)$$

We apply an SSM layer to obtain outputs  $\mathbf{U}_\ell$ :

$$\mathbf{U}_{1:L+1}^{(m)} = \text{SSM}(\bar{\mathbf{S}}^{(m)}), \quad (7)$$

where  $\mathbf{U}_{1:L+1}^{(m)}$  denotes the SSM outputs for all embeddings. In our implementation,  $\text{SSM}(\cdot)$  follows a Mamba-style selective SSM [12], enabling causal computation and efficient long-range dependency modeling.

We use the output of the system embedding,  $\mathbf{U}_{L+1}$ , to extract system-aware properties for routing. A router produces mixture weights over  $P$  experts via a softmax gate:

$$\mathbf{w} = \text{Softmax}(\text{Router}(\mathbf{U}_{L+1})) \in \mathbb{R}^P. \quad (8)$$

Given the output  $\mathbf{U}_{1:L}^{(m)}$ , the Sys-MoE block outputs  $\mathbf{Y}_{1:L}^{(m)}$  is computed as a weighted combination of expert predictions:

$$\mathbf{Y}_{1:L}^{(m)} = \sum_{p=1}^P w_p E_p(\mathbf{U}_{1:L}^{(m)}), \quad (9)$$

where  $w_p$  is the  $p$ -th entry of  $\mathbf{w}$ , and each expert  $E_p(\cdot)$  is implemented as an MLP. Finally, we stack multiple Sys-MoE blocks to increase expressivity for complex system dynamics.

#### 4.4 Objective Function.

After stacking *Sys-MoE Blocks*, we obtain the per-channel output sequence  $\mathbf{Y}_{1:L}^{(m)}$ . We apply a linear decoder head to produce logits over  $K$  uniform bins. Concretely, for each channel  $m$  outputs, we compute

$$\mathbf{P}_L^{(m)} = \text{Softmax}(\mathbf{W}_{\text{dec}} \mathbf{Y}_{1:L}^{(m)}) \in [0, 1]^K. \quad (10)$$

We train the model with a next-token cross-entropy loss on the state channels to match the categorical representation of the inputs:

$$\mathcal{L}_{\text{CE}} = - \sum_{\ell=1}^{L-1} \sum_{m=1}^{M_s} \phi(x_{\ell+1}^{(m)})^\top \log \mathbf{P}_\ell^{(m)}. \quad (11)$$

During inference time, we run the model in a *sequence-to-sequence manner*, enabling multi-step prediction in a single forward pass.

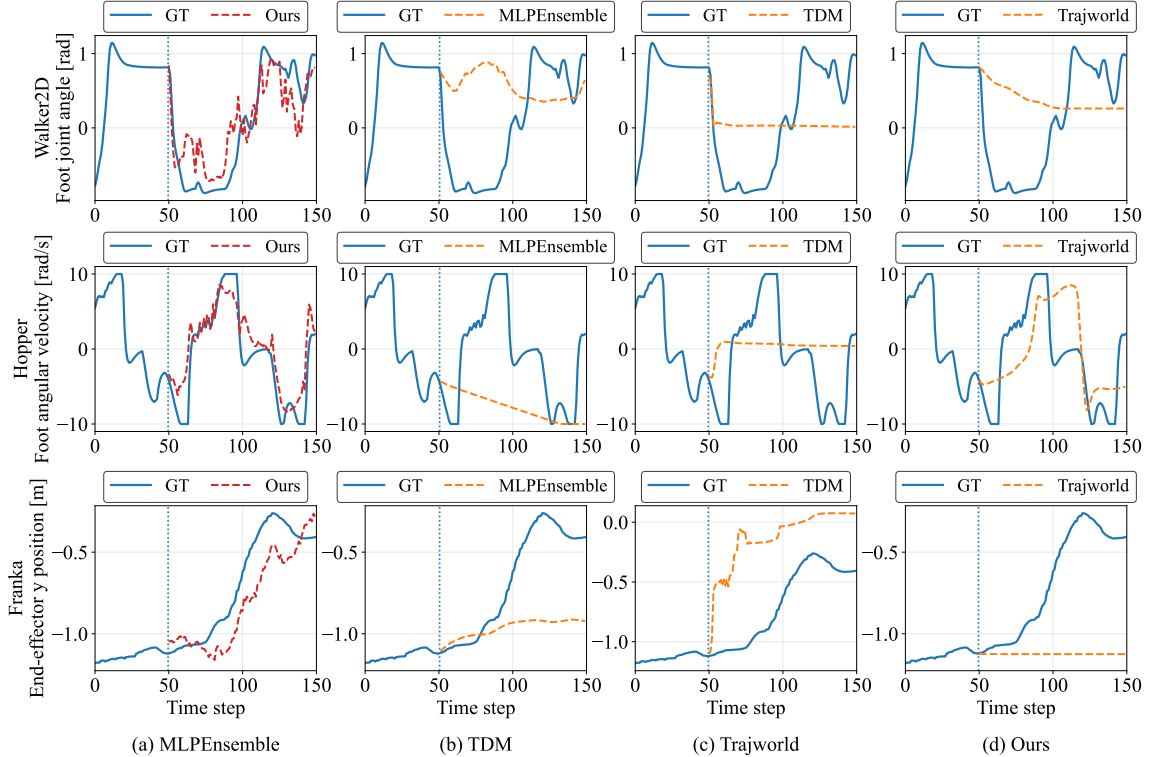


Figure 2: Trajectory plot comparison of our method and three baselines for 100-step rollout prediction on three robots: *Walker2D* foot joint angle, *Hopper* foot angular velocity, and *Franka* end-effector  $y$  position, given a 50-step history window as input. We can observe that our method tracks the ground-truth dynamics substantially more closely than the baselines over the 100-step horizon.

## 5 Experiments

In this section, we pretrain WestWorld on large-scale, diverse robotic datasets and conduct extensive experiments to evaluate: (i) zero-shot generalization to unseen environments, (ii) few-shot adaptation under domain shifts, (iii) scalability as the number of pretraining environments increases, and (iv) improvements in downstream control tasks across diverse robotic systems enabled by pretraining.

**Diverse Pretraining Datasets.** For pretraining the proposed trajectory world model, we collect a large amount of simulated and real-world data: i) UniTraj dataset [46], which contains 80 simulated robotic environments; and ii) 9 real-world robot-arm datasets from the Open X-Embodiment [38]. A detailed list of the pretraining and evaluation environments used in our experiments is provided in Appendix C.

**Baseline Methods.** We compare our method against several state-of-the-art trajectory world models. (1) *MLP Ensemble* [8]: a widely used baseline in model-based RL for learning probabilistic dynamics through an ensemble of multilayer perceptrons. (2) *TDM* [33]: a Transformer-based model built upon the Gato architecture, which flattens spatial and temporal features into a single sequence and applies one-dimensional attention for autoregressive prediction. (3) *TrajWorld* [46]: a Transformer-based trajectory model that employs temporal-variate attention for autoregressive rollout.

**Implementation Details.** We follow each baseline’s original pretraining configuration. Detailed training and implementation settings for WestWorld and all baselines are provided in Appendix D. For fairness, all baseline models are pretrained from scratch on the above same dataset as the proposed WestWorld.

### 5.1 Main Results

**Evaluation on Zero-shot Performance.** We first evaluate the zero-shot performance of our model on three unseen robotic environments that share similar structural morphology with those in the pretraining data. Specifically, we use datasets from three environments as our testbeds. These include *Hopper* and *Walker2D* from D4RL [10], as well as a *real-world* dataset of a mobile *Franka* manipulator interacting with articulated objects [32]. We evaluate 100-step

Table 1: Zero-shot generalization performance of different models on three dynamical systems. Errors are computed in the normalized space and reported as MAE and MSE ( $\times 10^{-2}$ ); lower is better.

Method	Walker2d ( $\times 10^{-2}$ )		Hopper ( $\times 10^{-2}$ )		Franka ( $\times 10^{-2}$ )	
	MAE ↓	MSE ↓	MAE ↓	MSE ↓	MAE ↓	MSE ↓
MLPEnsemble	26.006	12.028	19.987	7.216	12.164	4.271
TDM	20.122	6.428	17.634	5.076	23.686	8.435
Trajworld	22.261	8.623	17.388	5.441	13.102	5.127
Ours	<b>16.350</b>	<b>5.064</b>	<b>13.731</b>	<b>3.368</b>	<b>7.737</b>	<b>2.539</b>

Table 2: Few-shot generalization performance on three robotic systems. Results are computed in the normalized space and reported as MAE and MSE ( $\times 10^{-2}$ ) averaged over three random seeds (mean  $\pm$  standard deviation); lower is better.

Method	Cassie ( $\times 10^{-2}$ )		A1 ( $\times 10^{-2}$ )		UR5 ( $\times 10^{-2}$ )	
	MAE ↓	MSE ↓	MAE ↓	MSE ↓	MAE ↓	MSE ↓
MLPEnsemble	14.369 $\pm$ 0.523	4.416 $\pm$ 0.368	14.357 $\pm$ 1.009	3.707 $\pm$ 0.523	15.181 $\pm$ 0.597	4.936 $\pm$ 0.322
TDM	14.510 $\pm$ 0.642	3.404 $\pm$ 0.300	10.624 $\pm$ 0.312	2.151 $\pm$ 0.109	18.578 $\pm$ 0.324	5.510 $\pm$ 0.175
Trajworld	7.834 $\pm$ 0.167	1.697 $\pm$ 0.109	5.138 $\pm$ 0.200	0.900 $\pm$ 0.050	8.066 $\pm$ 0.799	2.117 $\pm$ 0.433
Ours	<b>5.316 <math>\pm</math> 0.108</b>	<b>0.808 <math>\pm</math> 0.025</b>	<b>4.227 <math>\pm</math> 0.120</b>	<b>0.628 <math>\pm</math> 0.040</b>	<b>4.925 <math>\pm</math> 0.317</b>	<b>0.831 <math>\pm</math> 0.150</b>

consecutive predictions using a 50-step history window as input. Mean Absolute Error (MAE) and Mean Squared Error (MSE) are used to assess the accuracy of long-horizon prediction.

As shown in Table 1, our method achieves the best performance across all three unseen environments in long-horizon prediction. This improvement is attributed to the combination of our system-aware MoE architecture and the structural inductive bias introduced through morphology-aware design. The MoE design enables the model to learn distinct dynamics for different morphologies while mitigating task interference during pretraining. In addition, we visualize trajectory plots for all three robots in Fig. 2. We can see that WestWorld tracks the ground-truth dynamics substantially more closely than the baselines over the 100-step horizon. The reason is that, in a zero-shot setting on unseen but structurally similar systems, our model selects appropriate experts to produce accurate dynamics predictions, whereas baseline methods lack morphology-aware representations and fail to generalize.

**Evaluation on Few-shot Adaptation.** To examine the benefits of pretraining for learning distinct robotic dynamics under limited data, we also evaluate few-shot performance on three *real-world datasets* that exhibit a significant domain gap from the pretraining distribution: i) Cassie bipedal jumping [1], ii) Unitree A1 quadruped locomotion [36], and iii) UR5 tabletop manipulation [47]. For each dataset, we fine-tune using only 10 episodes, employ early stopping based on performance on a validation split, and report MAE and MSE on held-out test trajectories.

We can see from Table 2 that our method consistently outperforms all baselines across the three robotic systems despite the large morphology and dynamics gap from the pretraining data. This demonstrates that the pretrained model provides a strong initialization and improves performance even when adapting to systems with substantial domain differences.

To further quantify the impact of pretraining, we compare few-shot learning curves of WestWorld with and without pretraining. Overall, pretraining significantly improves final prediction accuracy across all three robots. Detailed results are provided in Appendix E.

**Evaluation on Scalability.** We further verify the scalability of our method by varying the number of robotic environments while keeping the data budget per environment fixed. Specifically, we pretrain the model on  $N \in \{1, 2, 5, 10, 20, 30\}$  environments. The detailed task-level environment information is presented in Appendix C.4. For each environment, we use 1000 episodes for training, 500 episodes

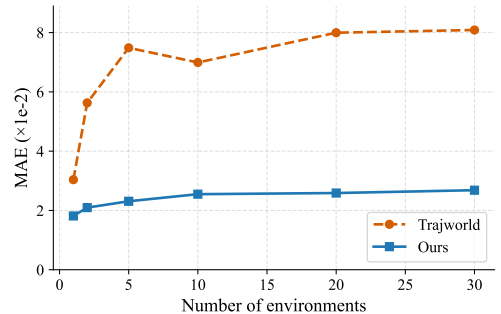


Figure 3: Comparison between our method against the best performing SOTA by scaling the number of environments.

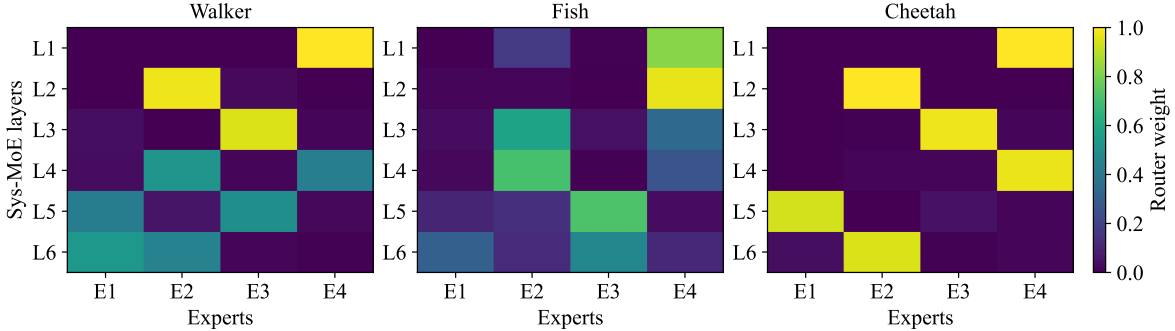


Figure 4: Sys-MoE routing weights across six layers (L1–L6), each containing four experts (E1–E4), for three robotic systems. Color indicates the router weight, where brighter values correspond to higher expert activation. The router exhibits near-sparse, system-dependent expert specialization, suggesting that different systems are modeled by different combinations of experts to capture their distinct dynamics.

for validation, and 500 episodes for testing. We compare the performance of our method with the state-of-the-art TrajWorld using test data.

All models take a 50-step history window as input and produce 100-step consecutive predictions. Fig. 3 reports the long-horizon prediction errors at each  $N$  environments. We observe that the accuracy of our method remains low and does not vary significantly with increasing  $N$ . The results show that our method can simultaneously learn distinct system dynamics across diverse environments. Conversely, TrajWorld’s performance degrades significantly as the number of environments increases. A plausible explanation is that optimizing a single shared model across multiple dissimilar dynamics exacerbates gradient interference and negative transfer, thereby limiting scalability [6].

To further analyze scalability, we visualize Sys-MoE routing weights for three distinct systems in Fig. 4. Across systems, the router exhibits sparse, system-dependent expert selection. These results support our key insight: complex dynamics can be effectively approximated by composing a set of basis dynamics modules with system-dependent coefficients. Such system-aware design mitigates interference in multi-system joint learning and enables scalable pretraining across diverse robotic systems.

Table 3: Downstream model-based control performance using MPPI on Walker2D, Hopper, and Unitree Go1. We report accumulated episode reward (higher is better) averaged over the evaluation episodes. All methods are evaluated with fixed random seeds and identical MPPI hyperparameters for fair comparison.

Method	Pretrain	Walker2d	Hopper	Go1
		Accumulate Reward $\uparrow$	Accumulate Reward $\uparrow$	Accumulate Reward $\uparrow$
MLPEnsemble	$\times$	119.18	147.37	-1.07
	$\checkmark$	190.51	200.56	-0.31
TDM	$\times$	122.65	242.34	-0.72
	$\checkmark$	207.61	154.64	0.03
Trajworld	$\times$	395.23	366.26	0.05
	$\checkmark$	1933.52	534.32	0.49
Ours	$\times$	707.61	554.92	0.43
	$\checkmark$	<b>2134.60</b>	<b>2253.51</b>	<b>2.20</b>

**Evaluation on Downstream Control Task.** In addition, we evaluate whether pretraining improves downstream model-based control across diverse robotic systems, which aims to isolate the effect of pretraining on dynamics modeling. Jointly optimizing the controller or policy is a separate question and is not considered here. We consider three robotic systems with distinct dynamics: Walker2D, Hopper from OpenAI Gym [37], and Unitree Go1 [3]. For each system, we collect an offline trajectory dataset from the environment. We then compare two training regimes for each world model: (i) fine-tuning from a pretrained checkpoint and (ii) training from scratch under the same dataset. After training, we deploy the learned dynamics model within MPPI [42], a commonly used sampling-based MPC controller. Additional details of the MPPI implementation are provided in Appendix D.3.

We set the MPPI planning horizon to 100 for Walker2D and Hopper, and to 40 for Go1. The setting is challenging: MPPI relies on long-horizon rollouts, so small model errors can compound and degrade control. In addition, the planner may explore actions that push the system outside the offline training distribution, further causing compounding errors and suboptimal control [27].

Table 3 reports the accumulated episode reward. We draw two key observations. First, for nearly all methods and systems, pretraining consistently improves control performance compared with training from scratch. This suggests that pretraining yields dynamics representations that generalize better under distribution shift between offline training and online MPC rollouts. Second, WestWorld achieves the best performance across all three systems under both training regimes, with particularly large gains after pretraining. This indicates that our scalable model design and morphology-informed inductive bias significantly improve downstream control performance.

Additionally, we conduct a **real-world deployment** on the Unitree Go1 by distilling WestWorld into a smaller student model and then fine-tuning it using simulated data. Due to real-world safety constraints and deployment costs, we only deploy WestWorld on the physical Go1 platform. All baselines fail to achieve stable locomotion in our simulation control setup, and we therefore do not consider them for real-world deployment.

The distilled-and-fine-tuned student world model is used as the dynamics predictor inside MPPI and successfully completes the real-world Go1 task of walking straight. This setting is particularly challenging because MPPI relies on long-horizon rollouts, where small model errors can compound and degrade control performance. In addition, the world model is trained purely in simulation, and sim-to-real gaps (e.g., actuator and contact dynamics, ground friction, battery-dependent torque limits, and state-estimation noise) can further increase rollout errors and lead to suboptimal control. Despite these challenges, our deployment uses only an offline simulation dataset for training and completes the walking task (Fig. 5), indicating that pretraining provides generalized dynamics learning benefits that can be transferred to real-world execution. A demo video is available at <https://westworldrobot.github.io/>. Details are provided in Appendix G.

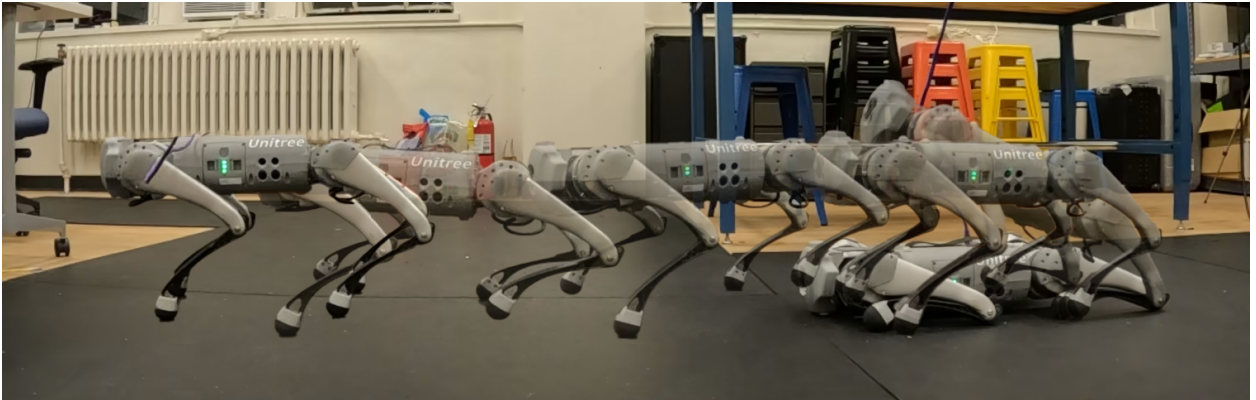


Figure 5: Real-world deployment on Unitree Go1. The distilled-and-fine-tuned WestWorld serves as the dynamics predictor in MPPI and enables the robot to walk straight toward the target goal.

## 5.2 Ablation Studies

We also explore the impact of two core components on model performance: 1) knowledge-encoded embedding (KNEE) modular and 2) system-aware Mixture-of-Experts (Sys-MoE) layer. Both ablation studies are performed during pretraining and subsequently evaluated under the same zero-shot experimental setting using three robotic systems: *Hopper*, *Walker2D*, and *Franka*. We report long-horizon dynamics prediction errors using MAE and MSE.

**Effect of the KNEE Modular.** To isolate the role of structural inductive bias, we remove the knowledge-encoded structural embedding during pretraining (denoted as “w/o structural embedding”). As shown in Table 4, removing structural embedding leads to a clear degradation on *Hopper* and *Walker2D*, which have more complex morphologies, while the drop on *Franka* is smaller. This results show that structural embedding is particularly beneficial for unseen complex robotic systems, where explicitly modeling physical connectivity helps align trajectory representations with system structure and improves zero-shot generalization.

**Effect of the Sys-MoE Layer.** To assess the importance of the Sys-MoE layer, we replace it with a dense SSM layer. For a fair comparison, we increase the depth of the dense-SSM variant so that its total number of parameters is comparable to that of our model. As shown in Table 4, this replacement degrades performance across tasks despite comparable model capacity. These results indicate that the Sys-MoE design is critical for jointly modeling diverse robotic dynamics, as it mitigates inter-task interference during multi-system training.

Based on the ablation study, we conclude that both KNEE and Sys-MoE are essential for model generalization and scalable pretraining.

Table 4: Ablation results under the zero-shot setting. We ablate the Sys-MoE layer by replacing it with a dense SSM, and ablate the structural encoding by removing it during pretraining. Results are computed in the normalized space and reported as MAE and MSE ( $\times 10^{-2}$ ); lower is better.

Method	Sys-MoE	Structural embedding	Walker2D ( $\times 10^{-2}$ )		Hopper ( $\times 10^{-2}$ )		Franka ( $\times 10^{-2}$ )	
			MAE ↓	MSE ↓	MAE ↓	MSE ↓	MAE ↓	MSE ↓
Ours w/o Sys-MoE	✗	✓	18.707	6.797	15.978	4.630	9.392	2.873
Ours w/o Structural embedding	✓	✗	21.156	7.872	16.227	4.990	7.897	2.707
Ours	✓	✓	<b>16.350</b>	<b>5.064</b>	<b>13.731</b>	<b>3.368</b>	<b>7.737</b>	<b>2.539</b>

### 5.3 Discussion

We also study parameter-efficient fine-tuning and provide a detailed inference-time latency comparison against autoregressive transformer baselines. Detailed analyses are deferred to Appendix F.

## 6 Conclusion and Limitation

In this work, we introduced WestWorld, a knowledge-encoded scalable trajectory world model designed for diverse robotics dynamics. Specifically, the proposed model leverages a Sys-MoE block to scale across diverse robotics dynamics and integrates morphology-aware structural embeddings to improve generalization ability. Extensive experimental results show that it significantly improves zero- and few-shot prediction performance on unseen robotic systems, enhances model scalability, as well as boosts downstream model-based control performance.

Despite its remarkable performance, WestWorld currently focuses on trajectory modeling and does not explicitly incorporate visual observations. In the future, we will extend WestWorld into a multimodal world model that fuses both vision and trajectory signals.

## Impact Statement

This paper aims to develop a general-purpose world model for diverse robotic systems to support prediction and control tasks. The proposed approach will significantly enhance the reliability and generalization of robotic systems operating in complex and dynamic environments. Beyond its technical contributions, this project is expected to catalyze interdisciplinary research at the intersection of machine learning, robotic systems, and control theory. Ultimately, it will facilitate the deployment of intelligent robotics in real-world applications, delivering broad benefits to both the research community and society.

## References

- [1] B. Acosta, W. Yang, and M. Posa. Validating robotics simulators on real-world impacts. *IEEE Robotics and Automation Letters*, 7(3):6471–6478, 2022.
- [2] N. Agarwal, A. Ali, M. Bala, Y. Balaji, E. Barker, T. Cai, P. Chattopadhyay, Y. Chen, Y. Cui, Y. Ding, et al. Cosmos world foundation model platform for physical ai. *arXiv preprint arXiv:2501.03575*, 2025.
- [3] J. Alvarez-Padilla, J. Z. Zhang, S. Kwok, J. M. Dolan, and Z. Manchester. Real-time whole-body control of legged robots with model-predictive path integral control. In *2025 IEEE International Conference on Robotics and Automation (ICRA)*, pages 14721–14727. IEEE, 2025.
- [4] S. Belkhale, Y. Cui, and D. Sadigh. Hydra: Hybrid robot actions for imitation learning. In *Conference on Robot Learning*, pages 2113–2133. PMLR, 2023.
- [5] L. Chen, S. Bahl, and D. Pathak. Playfusion: Skill acquisition via diffusion from language-annotated play. In *Conference on Robot Learning*, pages 2012–2029. PMLR, 2023.
- [6] Z. Chen, V. Badrinarayanan, C.-Y. Lee, and A. Rabinovich. Gradnorm: Gradient normalization for adaptive loss balancing in deep multitask networks. In *International conference on machine learning*, pages 794–803. PMLR, 2018.

- [7] X. Chi, P. Jia, C.-K. Fan, X. Ju, W. Mi, K. Zhang, Z. Qin, W. Tian, K. Ge, H. Li, et al. Wow: Towards a world omniscient world model through embodied interaction. *arXiv preprint arXiv:2509.22642*, 2025.
- [8] K. Chua, R. Calandra, R. McAllister, and S. Levine. Deep reinforcement learning in a handful of trials using probabilistic dynamics models. *Advances in neural information processing systems*, 31, 2018.
- [9] F. Ebert, C. Finn, S. Dasari, A. Xie, A. Lee, and S. Levine. Visual foresight: Model-based deep reinforcement learning for vision-based robotic control. *arXiv preprint arXiv:1812.00568*, 2018.
- [10] J. Fu, A. Kumar, O. Nachum, G. Tucker, and S. Levine. D4rl: Datasets for deep data-driven reinforcement learning. *arXiv preprint arXiv:2004.07219*, 2020.
- [11] Q. Gallouédec, E. Beeching, C. Romac, and E. Dellandréa. Jack of all trades, master of some, a multi-purpose transformer agent. *arXiv preprint arXiv:2402.09844*, 2024.
- [12] A. Gu and T. Dao. Mamba: Linear-time sequence modeling with selective state spaces. In *First conference on language modeling*, 2024.
- [13] C. Gulcehre, Z. Wang, A. Novikov, T. Paine, S. Gómez, K. Zolna, R. Agarwal, J. S. Merel, D. J. Mankowitz, C. Paduraru, et al. RL unplugged: A suite of benchmarks for offline reinforcement learning. *Advances in neural information processing systems*, 33:7248–7259, 2020.
- [14] Y. Guo, L. X. Shi, J. Chen, and C. Finn. Ctrl-world: A controllable generative world model for robot manipulation. *arXiv preprint arXiv:2510.10125*, 2025.
- [15] A. Gupta, S. Tian, Y. Zhang, J. Wu, R. Martín-Martín, and L. Fei-Fei. Maskvit: Masked visual pre-training for video prediction. *arXiv preprint arXiv:2206.11894*, 2022.
- [16] D. Ha and J. Schmidhuber. World models.
- [17] D. Ha and J. Schmidhuber. Recurrent world models facilitate policy evolution. *Advances in neural information processing systems*, 31, 2018.
- [18] N. Hansen, H. Su, and X. Wang. Td-mpc2: Scalable, robust world models for continuous control. In *The Twelfth International Conference on Learning Representations*, 2024.
- [19] N. Hansen, X. Wang, and H. Su. Temporal difference learning for model predictive control. In *International Conference on Machine Learning*, PMLR, 2022.
- [20] M. Heo, Y. Lee, D. Lee, and J. J. Lim. Furniturebench: Reproducible real-world benchmark for long-horizon complex manipulation. *The International Journal of Robotics Research*, 44(10-11):1863–1891, 2025.
- [21] G. Hinton, O. Vinyals, and J. Dean. Distilling the knowledge in a neural network. *arXiv preprint arXiv:1503.02531*, 2015.
- [22] S. Hong, D. Yoon, and K.-E. Kim. Structure-aware transformer policy for inhomogeneous multi-task reinforcement learning. In *International Conference on Learning Representations*, 2021.
- [23] W. Huang, I. Mordatch, and D. Pathak. One policy to control them all: Shared modular policies for agent-agnostic control. In *International Conference on Machine Learning*, pages 4455–4464. PMLR, 2020.
- [24] M. A. Lee, Y. Zhu, K. Srinivasan, P. Shah, S. Savarese, L. Fei-Fei, A. Garg, and J. Bohg. Making sense of vision and touch: Self-supervised learning of multimodal representations for contact-rich tasks. In *2019 International conference on robotics and automation (ICRA)*, pages 8943–8950. IEEE, 2019.
- [25] H. Liu, S. Nasiriany, L. Zhang, Z. Bao, and Y. Zhu. Robot learning on the job: Human-in-the-loop autonomy and learning during deployment. *The International Journal of Robotics Research*, 44(10-11):1727–1742, 2025.
- [26] X. Long, Q. Zhao, K. Zhang, Z. Zhang, D. Wang, Y. Liu, Z. Shu, Y. Lu, S. Wang, X. Wei, et al. A survey: Learning embodied intelligence from physical simulators and world models. *arXiv preprint arXiv:2507.00917*, 2025.
- [27] A. Parthasarathy, N. Kalra, R. Agrawal, Y. LeCun, O. Bounou, P. Izmailov, and M. Goldblum. Closing the train-test gap in world models for gradient-based planning. *arXiv preprint arXiv:2512.09929*, 2025.
- [28] A. Paszke, S. Gross, F. Massa, A. Lerer, J. Bradbury, G. Chanan, T. Killeen, Z. Lin, N. Gimelshein, L. Antiga, et al. Pytorch: An imperative style, high-performance deep learning library. *Advances in neural information processing systems*, 32, 2019.
- [29] M. H. Raibert, H. B. Brown Jr, M. Chepponis, J. Koechling, and J. K. Hodgins. Dynamically stable legged locomotion. Technical report, 1989.
- [30] A. Sawhney, S. Lee, K. Zhang, M. Veloso, and O. Kroemer. Playing with food: Learning food item representations through interactive exploration. In *International Symposium on Experimental Robotics*, pages 309–322. Springer, 2020.

- [31] S. Saxena, M. Sharma, and O. Kroemer. Multi-resolution sensing for real-time control with vision-language models. In *Conference on Robot Learning*, pages 2210–2228. PMLR, 2023.
- [32] G. Schiavi, P. Wulkop, G. Rizzi, L. Ott, R. Siegwart, and J. J. Chung. Learning agent-aware affordances for closed-loop interaction with articulated objects. In *2023 IEEE International Conference on Robotics and Automation (ICRA)*, pages 5916–5922. IEEE, 2023.
- [33] I. Schubert, J. Zhang, J. Bruce, S. Bechtle, E. Parisotto, M. Riedmiller, J. T. Springenberg, A. Byravan, L. Hasenclever, and N. Heess. A generalist dynamics model for control. *arXiv preprint arXiv:2305.10912*, 2023.
- [34] W. J. Schwind. *Spring loaded inverted pendulum running: A plant model*. University of Michigan, 1998.
- [35] R. Sekar, O. Rybkin, K. Daniilidis, P. Abbeel, D. Hafner, and D. Pathak. Planning to explore via self-supervised world models. In *International conference on machine learning*, pages 8583–8592. PMLR, 2020.
- [36] Y. Tang, W. Yu, J. Tan, H. Zen, A. Faust, and T. Harada. Saytap: Language to quadrupedal locomotion. In *7th Annual Conference on Robot Learning*.
- [37] M. Towers, A. Kwiatkowski, J. Terry, J. U. Balis, G. De Cola, T. Deleu, M. Goulão, A. Kallinteris, M. Krimmel, A. KG, et al. Gymnasium: A standard interface for reinforcement learning environments. *arXiv preprint arXiv:2407.17032*, 2024.
- [38] Q. Vuong, S. Levine, H. R. Walke, K. Pertsch, A. Singh, R. Doshi, C. Xu, J. Luo, L. Tan, D. Shah, et al. Open x-embodiment: Robotic learning datasets and rt-x models. In *Towards Generalist Robots: Learning Paradigms for Scalable Skill Acquisition@ CoRL2023*, 2023.
- [39] Y. Wang, H. Zhao, H. Lin, E. Xu, L. He, and H. Shao. A generalizable physics-enhanced state space model for long-term dynamics forecasting in complex environments. In *Forty-second International Conference on Machine Learning*, 2025.
- [40] S. Wei, X. Chen, F. Xie, G. E. Katz, Z. Gan, and L. Gan. Ms-ppo: Morphological-symmetry-equivariant policy for legged robot locomotion. *arXiv preprint arXiv:2512.00727*, 2025.
- [41] Y. Wen, Z. Wan, M. Zhou, S. Hou, Z. Cao, C. Le, J. Chen, Z. Tian, W. Zhang, and J. Wang. On realization of intelligent decision-making in the real world: A foundation decision model perspective. *arXiv preprint arXiv:2212.12669*, 2022.
- [42] G. Williams, A. Aldrich, and E. Theodorou. Model predictive path integral control using covariance variable importance sampling. *arXiv preprint arXiv:1509.01149*, 2015.
- [43] P. Wu, A. Escontrela, D. Hafner, P. Abbeel, and K. Goldberg. Daydreamer: World models for physical robot learning. In *Conference on robot learning*, pages 2226–2240. PMLR, 2023.
- [44] F. Xie, S. Wei, Y. Song, Y. Yue, and L. Gan. Morphological-symmetry-equivariant heterogeneous graph neural network for robotic dynamics learning. In *7th Annual Learning for Dynamics & Control Conference*, pages 1392–1405. PMLR, 2025.
- [45] D. Yarats, D. Brandfonbrener, H. Liu, M. Laskin, P. Abbeel, A. Lazaric, and L. Pinto. Don’t change the algorithm, change the data: Exploratory data for offline reinforcement learning. *arXiv preprint arXiv:2201.13425*, 2022.
- [46] S. Yin, J. Wu, S. Huang, X. Su, X. He, J. HAO, and M. Long. Trajectory world models for heterogeneous environments. In *Forty-second International Conference on Machine Learning*, 2025.
- [47] Y. Zhou, S. Sonawani, M. Phielipp, H. Ben Amor, and S. Stepputtis. Learning modular language-conditioned robot policies through attention. *Autonomous Robots*, 47(8):1013–1033, 2023.
- [48] F. Zhu, H. Wu, S. Guo, Y. Liu, C. Cheang, and T. Kong. Irasim: A fine-grained world model for robot manipulation. In *Proceedings of the IEEE/CVF International Conference on Computer Vision*, pages 9834–9844, 2025.
- [49] X. Zhu, R. Tian, C. Xu, M. Huo, W. Zhan, M. Tomizuka, and M. Ding. Fanuc manipulation: A dataset for learning-based manipulation with fanuc mate 200id robot, 2023.

## A Notations

The table below summarizes the notation used in this paper. Lowercase letters (e.g.,  $x$ ) denote scalars, bold lowercase letters (e.g.,  $\mathbf{x}$ ) represent vectors, and bold uppercase letters (e.g.,  $\mathbf{A}$ ,  $\mathbf{B}$ ) denote matrices.

Table 5: Summary of notations

Notation	Definition
$\mathcal{S}$	state space
$\mathcal{A}$	action space
$s$	state
$\mathbf{a}$	action
$n \in \mathbb{N}^+$	number of robotics systems
$N$	number of task-level environments in scalability evaluation
$\mathcal{D}_n$	trajectory data for $n$ -th robotics system
$h \in \mathbb{N}^+$	history state time steps
$k \in \mathbb{N}^+$	predicted future time steps
$m \in \mathbb{N}^+$	channel index
$x_t^{(m)} \in \mathbb{R}$	$m$ -th channel states or actions at time $t$
$\phi: \mathbb{R} \rightarrow \mathbb{R}^K$	discrete function
$z_t^{(m)} \in \mathbb{R}^d$	token embedding
$e_{\text{time}} \in \mathbb{R}^d$	timestep embedding
$e_{\text{ch}} \in \mathbb{R}^d$	channel order index embedding
$e_{\text{type}} \in \mathbb{R}^d$	modality embedding
$\mathbf{S}_t \in \mathbb{R}^{M_s \times d}$	state embedding at time $t$ , where $M_s$ denote the number of state channel
$\mathbf{A}_t \in \mathbb{R}^{M_a \times d}$	action embedding at time $t$ , where $M_a$ denote the number of action channel
$\pi_{\text{obj}}^i \in \mathbb{N}^+$	$i$ -th object index
$\pi_{\text{pre}}^{i,j} \in \mathbb{N}^+$	pre-order index for object $i$ and its body node $j$
$\pi_{\text{in}}^{i,j} \in \mathbb{N}^+$	in-order index for object $i$ and its body node $j$
$\pi_{\text{post}}^{i,j} \in \mathbb{N}^+$	post-order index for object $i$ and its body node $j$
$\mathbf{p} \in \mathbb{R}^d$	structural embedding
$\mathbf{q}_t \in \mathbb{R}^d$	query embedding at time $t$
$\tilde{\mathbf{S}}_t \in \mathbb{R}^{M_s \times d}$	state hidden states after state self-attention at time $t$
$\hat{\mathbf{S}}_t \in \mathbb{R}^{M_s \times d}$	state hidden states after action-state cross-attention at time $t$
$L \in \mathbb{N}^+$	the length after concatenating history states with queries
$\bar{\mathbf{S}}^{(m)} = [\hat{\mathbf{S}}_{1:L}^{(m)}; \mathbf{e}]$	state embedding concatenate with system embedding
$\mathbf{e} \in \mathbb{R}^d$	the learnable system embedding
$\mathbf{U}_\ell$	$l$ -th SSM output
$P \in \mathbb{N}^+$	the number of expert
$\mathbf{Y}_{1:L}^{(m)} \in \mathbb{R}^{L \times d}$	$m$ -th channel System-Aware MoE Block output
$\mathbf{P}_\ell^{(m)} \in \mathbb{R}^K$	categorical representation output
$M_s$	the number of state channels
$M_a$	the number of action channels
$K$	the number of categorical bins

## B A Walk-Through Example for Structural Embedding

This section provides a concrete example of how we construct the knowledge-encoded structural embedding in Eq. (3). We use the Walker robot as an illustrative example.

**Step 1: Extract the robot kinematic tree.** Given the Walker structural file (e.g., an MJCF or URDF specification), we extract the articulated-body hierarchy and treat it as a rooted kinematic tree. Walker contains a single articulated object (the robot itself), so we set  $\pi_{\text{obj}}^i = 0$ . The robot has seven body nodes: torso, right thigh, right leg, right foot, left thigh, left leg, and left foot.

**Step 2: LCRS conversion and traversal ranks.** We convert the rooted kinematic tree into a binary tree via the left-child-right-sibling (LCRS) transformation [22]. We then compute traversal ranks on the LCRS-converted binary tree, including pre-order, in-order, and post-order indices. For each body node  $j$ , we obtain a tuple of traversal ranks  $(\pi_{\text{pre}}^{0,j}, \pi_{\text{in}}^{0,j}, \pi_{\text{post}}^{0,j})$ . For Walker, the indices for all seven body nodes are listed in Table 6.

Table 6: Walker example of LCRS traversal ranks used to construct structural embeddings. Here  $\pi_{\text{obj}} = 0$  since the scene contains only the robot.

Body	Global idx	$\pi_{\text{pre}}$	$\pi_{\text{in}}$	$\pi_{\text{post}}$
torso	0	0	6	6
right_thigh	1	1	3	5
right_leg	2	2	5	4
right_foot	3	3	4	3
left_thigh	4	4	2	2
left_leg	5	5	1	1
left_foot	6	6	0	0

**Step 3: Construct per-body structural embeddings.** For each body node  $(i, j)$ , we form the discrete index tuple

$$(\pi_{\text{obj}}^i, \pi_{\text{pre}}^{i,j}, \pi_{\text{in}}^{i,j}, \pi_{\text{post}}^{i,j}),$$

which uniquely identifies the node in the LCRS-converted binary tree (and also disambiguates multiple objects when present). We embed each index using a lookup table and concatenate the results as in Eq. (3):

$$\mathbf{p}^{(i,j)} = \text{Concat}(e_{\text{obj}}(\pi_{\text{obj}}^i), e_{\text{pre}}(\pi_{\text{pre}}^{i,j}), e_{\text{in}}(\pi_{\text{in}}^{i,j}), e_{\text{post}}(\pi_{\text{post}}^{i,j})) \in \mathbb{R}^d.$$

Finally, we inject the structural prior by adding  $\mathbf{p}^{(i,j)}$  to the corresponding per-body token embedding (e.g., state/action/query tokens associated with body  $j$ ). This yields structure-aware trajectory embeddings that are consistent across morphologies.

## C Detailed Dataset Settings

In this appendix, we provide the detailed dataset settings in the experiments. This includes the datasets for pretraining, zero-shot evaluation, few-shot evaluation, scalability evaluation, and downstream model-based control.

### C.1 Pretraining Datasets

For pretraining the trajectory world model, we use both large-scale simulated and real-world data. Specifically, we use: (i) the UniTraj dataset [46], which aggregates trajectories from ExORL [45], RL Unplugged [13], JAT [11], DB-1 [41], TD-MPC2 [18], and Modular RL [23], covering in total 80 task-level simulated environments; and (ii) 9 real-world robot-arm datasets from Open X-Embodiment [38]. We first summarize the robot morphology categories in Table 7, and then list all 89 task-level environments used for pretraining in Table 8.

**Data preprocessing.** To stabilize training across heterogeneous robotic systems, we follow UniTraj [46] and apply channel-wise min-max normalization. For each robot and each feature dimension (e.g., joint position, joint velocity (angular or linear), or torque), we compute the empirical minimum and maximum values on the training split and rescale inputs to  $[0, 1]$ . Each trajectory segment is clipped or zero-padded to a maximum length of 150 time steps. Across all pretraining datasets, the maximum state dimension is 78 and the maximum action dimension is 21.

Table 7: A detailed list of diverse robotics used in the pretraining dataset. For robotics sharing the same name, we mark those from OpenAI Gym with an asterisk (\*) and those from DeepMind Control Suite with a dagger (†).

Dataset	Robot morphology categories
ExORL [45]	Cartpole, Jaco, Quadruped, Walker <sup>†</sup>
RL Unplugged [13]	Cartpole, Fish, Humanoid, Manipulator, Walker <sup>†</sup>
JAT [11]	Double Pendulum*, Pendulum*, Pusher*, Reacher*, Swimmer*
DB-1 [41]	Acrobat, Ball In Cup, Cartpole, Cheetah-2-back, Cheetah-2-front, Cheetah-3-back, Cheetah-3-balanced, Cheetah-3-front, Cheetah-4-allback, Cheetah-4-allfront, Cheetah-4-back, Cheetah-4-front, Cheetah-5-back, Cheetah-5-balanced, Cheetah-5-front, Cheetah-6-back, Cheetah-6-front, Finger, Fish, Hopper <sup>†</sup> , Hopper-3, Hopper-5, Humanoid, Humanoid-2d-7-left-arm, Humanoid-2d-7-left-leg, Humanoid-2d-7-lower-arms, Humanoid-2d-7-right-arm, Humanoid-2d-7-right-leg, Humanoid-2d-8-left-knee, Humanoid-2d-8-right-knee, Humanoid-2d-9-full, Manipulator, Reacher, Swimmer6, Swimmer15, Walker <sup>†</sup> , Walker-2-flipped, Walker-2-main, Walker-3-flipped, Walker-3-main, Walker-4-flipped, Walker-4-main, Walker-5-flipped, Walker-5-main, Walker-6-flipped, Walker-6-main
TD-MPC2 [18]	Acrobat, Ball In Cup, Cartpole, Cheetah <sup>†</sup> , Finger, Fish, Hopper <sup>†</sup> , Pendulum <sup>†</sup> , Reacher <sup>†</sup> , Walker <sup>†</sup>
Modular RL [23]	Cheetah-2-back, Cheetah-2-front, Cheetah-3-back, Cheetah-3-balanced, Cheetah-4-allback, Cheetah-4-back, Cheetah-4-front, Cheetah-5-back, Cheetah-5-balanced, Cheetah-5-front, Cheetah-6-back, Cheetah-6-front, Hopper-3, Hopper-5, Walker-2-flipped, Walker-3-flipped, Walker-4-flipped, Walker-5-flipped, Walker-6-flipped, Walker-7-flipped
Open X-Embodiment [38]	Fanuc Mate 6-DoF industrial arm [49], KUKA iiwa 7-DoF arm [24], Franka Emika Panda arm [20], Franka arm [4, 25, 31, 30, 5], Sawyer arm [15].

### C.2 Zero-shot experiment datasets.

To evaluate zero-shot generalization, we consider three unseen environments: *Walker2D* and *Hopper* from OpenAI Gym [37], and a real-world dataset of a mobile *Franka* manipulator interacting with articulated objects [32]. None of these systems appears during pretraining, but they share similar structural morphology with robots in the pretraining data, making them suitable for testing generalization to unseen environments.

For *Walker2D* and *Hopper*, we use expert demonstrations from D4RL [10] for evaluation. The *Walker2D* dataset contains 1,267 episodes, and the *Hopper* dataset contains 1,029 episodes. The mobile *Franka* dataset contains 118 episodes.

Table 8: Task-level environments used in the pretraining dataset.

Component	Task-level environments	#
TD-MPC2	walker-stand, walker-walk, walker-run, cheetah-run, reacher-easy, reacher-hard, acrobot-swingup, pendulum-swingup, cartpole-balance, cartpole-balance-sparse, cartpole-swingup, cartpole-swingup-sparse, cup-catch, finger-spin, finger-turn-easy, finger-turn-hard, fish-swim, hopper-stand, hopper-hop, walker-walk-backwards, walker-run-backwards, cheetah-run-backwards, cheetah-run-front, cheetah-run-back, cheetah-jump, hopper-hop-backwards, reacher-three-easy, reacher-three-hard, cup-spin, pendulum-spin	30
ExORL	jaco-reach, quadruped-locomotion	2
RL-Unplugged	humanoid_run, manipulator-insert-ball, manipulator-insert-peg	3
JAT	inverted_double_pendulum, inverted_pendulum, pusher, reacher, swimmer	5
DB-1	acrobot, cheetah_2_back, cheetah_2_front, cheetah_3_back, cheetah_3_balanced, cheetah_3_front, cheetah_4_allback, cheetah_4_allfront, cheetah_4_back, cheetah_4_front, cheetah_5_back, cheetah_5_balanced, cheetah_5_front, cheetah_6_back, cheetah_6_front, hopper_3, hopper_5, humanoid, humanoid_2d_7_left_arm, humanoid_2d_7_left_leg, humanoid_2d_7_lower_arms, humanoid_2d_7_right_arm, humanoid_2d_7_right_leg, humanoid_2d_8_left_knee, humanoid_2d_8_right_knee, humanoid_2d_9_full, manipulator-bring_ball, swimmer6, swimmer15, walker_2_flipped, walker_2_main, walker_3_flipped, walker_3_main, walker_4_flipped, walker_4_main, walker_5_flipped, walker_5_main, walker_6_flipped, walker_6_main	39
Modular-RL	walker_7_flipped	1
Open X-Embodiment	Fanuc-Mate-6DoF-tabletop-manipulation, KUKA-iiwa-7DoF-insertion, Franka-Emika-Panda-assemble-furniture, Franka-kitchen-manipulation, Franka-insertion, Franka-tabletop-manipulation, Franka-food-manipulation, Franka-play-with-object, Sawyer-pick-and-place	9
<b>Total</b>		<b>89</b>

### C.3 Few-shot experiment datasets.

To study few-shot adaptation under substantial domain shift, we evaluate on three real-world robotic datasets that are not covered by the pretraining distribution: (i) Cassie bipedal jumping [1], (ii) Unitree A1 quadruped locomotion [36], and (iii) UR5 tabletop manipulation [47]. All three datasets differ markedly from the simulated pretraining data in morphology and dynamics.

For each robot, we fine-tune WestWorld using only 10 training episodes, select the checkpoint via early stopping on a held-out validation split, and report MAE/MSE on a separate test split. UR5 provides 110 episodes in total, which we split into 10/50/50 for train/validation/test. Unitree A1 contains 20 episodes and is split into 10/5/5, and Cassie contains 28 episodes and is split into 10/6/12.

### C.4 Scaling of environmental datasets

In the environment-scaling study, we vary the number of pretraining environments and consider  $N \in \{1, 2, 5, 10, 20, 30\}$ . For each value of  $N$ , we train on the task-level environment subset listed in Table 9. Within each selected environment, we use the same fixed episode split: 1000 episodes for training, 500 episodes for validation, and 500 episodes for testing. As a result, the total numbers of training, validation, and test episodes increase proportionally with  $N$ .

### C.5 Downstream control task datasets.

In addition to trajectory prediction, we evaluate downstream model-based control using the learned WestWorld. We consider three robotic systems: Walker2D and Hopper from OpenAI Gymnasium [37], and the real-world Unitree Go1

Table 9: Detailed task-level environment subsets for the environment-scaling study. For each  $N$ , each environment uses a fixed split of 1000/500/500 episodes for train/val/test.

$N$	Selected task-level environments
1	Cartpole Swingup
2	Cartpole Swingup; Acrobot Swingup
5	Walker Walk Backwards; Finger Turn Easy; Cartpole Swingup; Reacher Three Easy; Cheetah Run Front
10	Walker Walk Backwards; Finger Turn Easy; Cartpole Swingup; Reacher Three Easy; Cheetah Run Front; Acrobot Swingup; Reacher Hard; Cup Catch; Cartpole Swingup Sparse; Finger Turn Hard
20	Walker Walk Backwards; Finger Turn Easy; Cartpole Swingup; Reacher Three Easy; Cheetah Run Front; Acrobot Swingup; Reacher Hard; Cup Catch; Cartpole Swingup Sparse; Finger Turn Hard; Cartpole Balance Sparse; Hopper Hop Backwards; Pendulum Spin; Cheetah Run Backwards; Fish Swim; Reacher Three Hard; Walker Walk; Finger Spin; Hopper Hop; Walker Run
30	Walker Walk Backwards; Finger Turn Easy; Cartpole Swingup; Reacher Three Easy; Cheetah Run Front; Acrobot Swingup; Reacher Hard; Cup Catch; Cartpole Swingup Sparse; Finger Turn Hard; Cartpole Balance Sparse; Hopper Hop Backwards; Pendulum Spin; Cheetah Run Backwards; Fish Swim; Reacher Three Hard; Walker Walk; Finger Spin; Hopper Hop; Walker Run; Hopper Stand; Cup Spin; Reacher Easy; Cheetah Jump; Pendulum Swingup; Cartpole Balance; Cheetah Run Back; Walker Stand; Cheetah Run; Walker Run Backwards

locomotion dataset [3]. For each system, we construct an offline dataset for learning the dynamics model from MPPI rollouts and then evaluate control performance by deploying MPPI online.

**MPPI rollout collection.** We run MPPI for 100 episodes per system. For Walker2D and Hopper, each episode has 1000 environment steps, with planning horizon  $H = 100$  and  $N = 256$  sampled action sequences per step. For Go1, each episode has 2000 steps, with planning horizon  $H = 40$  and  $N = 30$  sampled action sequences per step. The MPPI cost definition for each task is provided in Appendix D.3.

**Training/validation data construction.** At each time step, we rank the  $N$  sampled rollouts by MPPI cost and keep only the lowest-cost trajectories. Specifically, for training we retain the lowest 10% rollouts from the 100 MPPI episodes and use them as supervised targets for dynamics learning. To improve data diversity, we additionally include all sampled rollouts from 3 extra episodes as augmentation. For validation, we use 5 episodes and retain the lowest 30% rollouts at each time step for early stopping and model selection. For testing, we report test performance by running MPPI online in the corresponding environment using the learned world model for rollouts.

## D Detailed Experimental Settings

We present the detailed experimental settings in this Section. All pre-training experiments are conducted on a server equipped with 4 NVIDIA H200 GPUs, utilizing the PyTorch framework [28].

### D.1 Hyperparameters for Models

This subsection summarizes the model hyperparameters used in our experiments. For all baseline methods, we follow the official implementations and the hyperparameter choices reported in prior work [46, 33].

**TrajWorld.** We use a TrajWorld architecture with discretized prediction using 256 uniform bins. The model has 6 Transformer blocks and 4 attention heads, with dropout rate 0.1. The hidden dimension is set to 256. Each block uses an MLP with hidden sizes [1024, 256] and GeLU activation.

**TDM.** We use the TDM architecture with discretized prediction using 256 uniform bins. The model has hidden dimension 384, 6 Transformer blocks, and 4 attention heads, with dropout rate 0.1. Each block uses an MLP with hidden sizes [1536, 384] and GeLU activation.

**MLPEnsemble.** For MLPEnsemble, we train an ensemble of transition models parameterized as a diagonal Gaussian over the next state, implemented with MLPs and optimized by negative log-likelihood using bootstrapped training samples. We use 7 MLPs, each with four hidden layers of width 640 (i.e., [640, 640, 640, 640]), and select the top 5 *elite* models by validation loss. To handle heterogeneous systems, we pad state and action vectors to fixed sizes before concatenation, producing a fixed-dimensional input to the MLP.

**WestWorld.** Our model follows the same discretized prediction setup as TrajWorld, using 256 uniform bins. The backbone consists of 6 Sys-MoE blocks with 4 attention heads, hidden dimension 256, and dropout rate 0.1. Each block uses an MLP with hidden size 512 and GeLU activation. For the SSM module in our Sys-MoE layer, implemented with a Mamba-style state-space model using state size 64, convolution width 4, expansion factor 2. Unless otherwise noted, each Sys-MoE layer contains  $P = 4$  experts, which we select via validation as described below.

**Determining the number of experts.** Our Sys-MoE uses  $P$  experts per Sys-MoE layer, where  $P$  is a tunable hyperparameter. We select  $P$  using a held-out validation split from the pretraining data. Specifically, we randomly sample 1% of trajectories from the 89 pretraining environments as a validation set and exclude them from optimization. This split is used only for model selection and does not overlap with any test environments. We select  $P \in \{2, 4, 6, 8\}$  and report (i) the best validation MAE and (ii) the corresponding training step at which the best MAE is achieved (Table 10). While  $P = 8$  achieves the lowest validation MAE, it requires substantially more training (about  $1.6\times$  the steps of  $P = 4$ ), leading to higher computational cost. The improvement from  $P = 4$  to  $P = 8$  is relatively modest on this validation split. Therefore, we use  $P = 4$  as the default setting to balance accuracy and pretraining efficiency.

Table 10: Best validation MAE and the optimizer update step  $s^*$  at which the best MAE is achieved during pretraining. We report  $s^*$  in thousands of updates (k). MAE is computed in the normalized space. Lower values indicate better performance. † denotes the setting used in all experiments.

#Experts $P$	Val. MAE ↓	Best step $s^*$ (k updates)
2	0.0409	108.6
4†	0.0379	137.2
6	0.0390	176.7
8	0.0340	214.0

## D.2 Training and Evaluation Settings

Below, we summarize the training and evaluation details for all experiments.

**Pretraining settings:** For all baseline methods, we follow the original pretraining protocols reported in prior work [46, 33]. Specifically, for *TDM* and *TrajWorld*, we pretrain for a total of *up to* 1M gradient steps using the Adam optimizer with batch size 64 and learning rate  $1 \times 10^{-4}$ . We apply dropout with rate 0.05, weight decay  $1 \times 10^{-5}$ , and gradient clipping with norm 0.25. We use a warmup cosine decay learning-rate schedule with 10,000 warmup steps. For *MLPEnsemble*, we pretrain for *up to* 1M gradient steps with Adam, batch size 256, and learning rate  $1 \times 10^{-4}$ .

For our method, we pretrain for *up to* 1M gradient steps with AdamW, batch size 48, and learning rate  $2 \times 10^{-4}$ , while keeping dropout 0.05, weight decay  $1 \times 10^{-5}$ , gradient clipping norm 0.25, and the warmup cosine decay schedule with 10,000 warmup steps. Each training trajectory segment is clipped or zero-padded to a maximum length of 150 time steps. We use the first one-third of the segment (up to 50 steps) as the history window and predict the remaining future steps (up to 100 steps).

**Zero-shot evaluation settings:** We evaluate zero-shot long-horizon prediction on three *unseen* environments: *Walker2D* and *Hopper* from OpenAI Gym [37], and a real-world dataset of a mobile *Franka* manipulator interacting with articulated objects [32]. For each dataset, we split each episode into trajectory segments of length 150. For all methods, we use the first 50 time steps as the history input and autoregressively roll out the next 100 time steps. We report MAE and MSE by comparing the 100-step predictions against the ground-truth future trajectory.

**Few-shot training settings:** For all methods in the 10-episode fine-tuning experiments, we use the AdamW optimizer with learning rate  $1 \times 10^{-5}$  for up to 300 steps, with early stopping based on validation performance, and a maximum batch size of 12. Each training trajectory segment is clipped or zero-padded to a maximum length of 150 time steps. For the experiments that analyze pretraining benefits and quantify pretraining impact in Appendix E, we use AdamW with learning rate  $1 \times 10^{-4}$  for up to 1500 steps for the train-from-scratch setting, again with validation-based early stopping and maximum batch size 12.

**Few-shot evaluation settings:** We evaluate few-shot long-horizon prediction on three real-world datasets: (i) Cassie bipedal jumping [1], (ii) Unitree A1 quadruped locomotion [36], and (iii) UR5 tabletop manipulation [47]. For Unitree A1 and UR5, all methods take the first 50 time steps as the history input and roll out the next 100 time steps. For Cassie, we use the same 50-step history window but predict only the next 50 time steps due to the shorter episode length. We report MAE and MSE by comparing the predictions against the corresponding ground-truth future trajectories.

**Downstream control training settings:** For all methods trained on the control datasets, we use the AdamW optimizer with learning rate  $1 \times 10^{-5}$  for up to 50,000 steps, with early stopping based on validation performance, and a maximum batch size of 48. Each training trajectory segment is clipped or zero-padded to a maximum length of 100 time steps.

**Downstream control evaluation settings:** For control evaluation, we deploy each learned world model as the dynamics predictor within an MPPI controller. We set the prediction horizon to  $H = 100$  for *Walker2D* and *Hopper*, and to  $H = 40$  for *Unitree Go1*. At each control step, MPPI samples 256 candidate action sequences for *Walker2D/Hopper* and 30 for *Go1*, and uses the world model to roll out the corresponding trajectories for cost evaluation. All methods use identical MPPI hyperparameters for fair comparison, as detailed in Appendix D.3.

### D.3 Description of Planning Algorithm

This section summarizes the trajectory optimization procedure used in our downstream control evaluations. Across Walker2D, Hopper, and Unitree Go1, we use a sampling-based MPC method, *Model Predictive Path Integral* (MPPI) [42], to optimize an open-loop action sequence over a finite horizon using the learned world model. At each control cycle, MPPI samples candidate action sequences, rolls them out through the world model, evaluates their trajectory costs, and updates the nominal action sequence via an exponentially weighted average. The first action is then executed in a receding-horizon manner.

**MPPI with a learned world model.** Let  $f_\theta$  denote the learned dynamics model. Given the current state  $s_0$ , MPPI optimizes an action sequence  $\mathbf{a}_{0:H-1} = (\mathbf{a}_0, \dots, \mathbf{a}_{H-1})$  over a horizon  $H$  by rolling out

$$\mathbf{s}_{t+1} = f_\theta(\mathbf{s}_t, \mathbf{a}_t), \quad t = 0, \dots, H-1. \quad (12)$$

We maintain a nominal sequence  $\boldsymbol{\mu}_{0:H-1}$  and sample  $N$  perturbed sequences:

$$\mathbf{a}_t^{(n)} = \boldsymbol{\mu}_t + \boldsymbol{\epsilon}_t^{(n)}, \quad \boldsymbol{\epsilon}_t^{(n)} \sim \mathcal{N}(\mathbf{0}, \boldsymbol{\Sigma}), \quad n = 1, \dots, N, t = 0, \dots, H-1. \quad (13)$$

For each sample, we compute the trajectory cost

$$L^{(n)} = \sum_{t=0}^{H-1} \ell(\mathbf{s}_t^{(n)}, \mathbf{a}_t^{(n)}; \mathbf{s}_t^{\text{ref}}), \quad (14)$$

and assign importance weights using a temperature parameter  $\lambda$ :

$$w^{(n)} \propto \exp\left(-\frac{1}{\lambda}(L^{(n)} - L_{\min})\right), \quad L_{\min} = \min_n L^{(n)}, \quad \sum_{n=1}^N w^{(n)} = 1. \quad (15)$$

The nominal sequence is updated by the weighted average

$$\boldsymbol{\mu}_t \leftarrow \sum_{n=1}^N w^{(n)} \mathbf{a}_t^{(n)}, \quad t = 0, \dots, H-1. \quad (16)$$

We execute the first action  $\boldsymbol{\mu}_0$  and repeat this procedure at the next control cycle.

For consistent reporting across tasks, we evaluate control performance using *accumulated reward* (higher is better), which is specified for each task below.

#### D.3.1 Walker2D

**Task.** We consider forward walking in the Walker2D environment [37]. Let the Walker2D state at time  $t$  be  $\mathbf{s}_t$  and the control input be  $\mathbf{a}_t$ .

**Cost for forward walking.** We define the per-step cost as the negative of the standard Walker2D reward (i.e., lower cost corresponds to higher reward), following the Gymnasium formulation [37]:

$$\ell(\mathbf{s}_t, \mathbf{a}_t) = -\left(r_{\text{healthy}}(t) + r_{\text{fwd}}(t) - c_{\text{ctrl}}(t)\right), \quad (17)$$

where  $r_{\text{healthy}}(t)$  is a survival bonus when the walker remains healthy,  $r_{\text{fwd}}(t)$  measures forward progress, and  $c_{\text{ctrl}}(t)$  penalizes large control inputs.

Specifically, let  $x_t$  denote the walker horizontal position (root  $x$  coordinate) at time  $t$ , and let  $\Delta t$  be the simulation time step. The forward progress reward is computed from the root velocity:

$$r_{\text{fwd}}(t) = w_{\text{fwd}} \frac{x_{t+1} - x_t}{\Delta t}, \quad (18)$$

with  $w_{\text{fwd}} = 0.5$ , and the control cost is

$$c_{\text{ctrl}}(t) = w_{\text{ctrl}} \|\mathbf{a}_t\|_2^2, \quad (19)$$

with  $w_{\text{ctrl}} = 10^{-3}$ . The survival bonus is

$$r_{\text{healthy}}(t) = \begin{cases} 1, & \text{if the walker is healthy,} \\ 0, & \text{otherwise,} \end{cases} \quad (20)$$

where the health condition follows Gymnasium Walker2D and requires the state to remain within predefined ranges, including torso height  $z \in [0.8, 2.0]$  and torso angle  $\theta \in [-1.0, 1.0]$ .

To improve stability of MPPI planning, we additionally include an expert-reference tracking term defined in the state space using an expert trajectory from D4RL [10]:

$$\ell_{\text{ref}}(t) = (\mathbf{s}_t - \mathbf{s}_t^{\text{ref}})^\top \mathbf{Q} (\mathbf{s}_t - \mathbf{s}_t^{\text{ref}}), \quad (21)$$

where  $\mathbf{s}_t^{\text{ref}}$  is the reference state at time  $t$  and  $\mathbf{Q}$  is a diagonal weight vector. In our implementation, the reference is defined over the concatenated generalized positions and velocities  $(\mathbf{q}, \dot{\mathbf{q}})$ , and we use per-dimension weights

$$\mathbf{Q}_q = [0.0, 10.0, 10.0, 10.0, 1.0, 1.0, 10.0, 1.0, 1.0], \quad \mathbf{Q}_{\dot{q}} = [0.01, 0.01, 0.01, 0.01, 0.01, 0.01, 0.01, 0.01, 0.01],$$

where the first position weight is set to 0 to ignore the root  $x$  coordinate. We set  $\mathbf{Q} = [\mathbf{Q}_q; \mathbf{Q}_{\dot{q}}]$ .

Finally, the MPPI objective over horizon  $H$  is

$$L_{\text{walk}} = \sum_{t=0}^{H-1} (\ell(\mathbf{s}_t, \mathbf{a}_t) + \ell_{\text{ref}}(t)). \quad (22)$$

**Accumulated reward.** We report the episode-level accumulated reward using the standard Walker2D reward:

$$R_{\text{ep}} = \sum_{t=0}^{T-1} (r_{\text{healthy}}(t) + r_{\text{fwd}}(t) - c_{\text{ctrl}}(t)). \quad (23)$$

**MPPI parameters.** We use temperature  $\lambda = 0.25$ , horizon  $H = 100$ , and  $N = 256$  sampled trajectories per control cycle.

### D.3.2 Hopper

**Task.** We consider forward hopping in the Hopper environment [37]. Let the Hopper state at time  $t$  be  $\mathbf{s}_t$  and the control input be  $\mathbf{a}_t$ .

**Cost for forward hopping.** We define the per-step cost as the negative of the standard Hopper reward (i.e., lower cost corresponds to higher reward), following the Gymnasium formulation [37]:

$$\ell(\mathbf{s}_t, \mathbf{a}_t) = -(r_{\text{healthy}}(t) + r_{\text{fwd}}(t) - c_{\text{ctrl}}(t)), \quad (24)$$

where  $r_{\text{healthy}}(t)$  is a survival bonus when the hopper remains healthy,  $r_{\text{fwd}}(t)$  measures forward progress, and  $c_{\text{ctrl}}(t)$  penalizes large control inputs.

Specifically, let  $x_t$  denote the hopper’s horizontal position (root  $x$  coordinate) at time  $t$ , and let  $\Delta t$  be the simulation time step. The forward progress reward is

$$r_{\text{fwd}}(t) = \frac{x_{t+1} - x_t}{\Delta t}, \quad (25)$$

and the control cost is

$$c_{\text{ctrl}}(t) = w_{\text{ctrl}} \|\mathbf{a}_t\|_2^2, \quad (26)$$

with  $w_{\text{ctrl}} = 10^{-3}$ . The survival bonus is

$$r_{\text{healthy}}(t) = \begin{cases} 1, & \text{if the hopper is healthy,} \\ 0, & \text{otherwise,} \end{cases} \quad (27)$$

where the health condition follows Gymnasium Hopper and requires the state to remain within predefined ranges (e.g., torso height and angle).

To improve stability of MPPI planning, we additionally include an expert-reference tracking term defined in the position and velocity space using a expert trajectory from D4RL [10]:

$$\ell_{\text{ref}}(t) = (\mathbf{s}_t - \mathbf{s}_t^{\text{ref}})^\top \mathbf{Q} (\mathbf{s}_t - \mathbf{s}_t^{\text{ref}}), \quad (28)$$

where  $\mathbf{s}_t^{\text{ref}}$  is the reference state at time  $t$ , and  $\mathbf{Q}$  is a diagonal weight matrix with position and velocity weights. In our implementation, we set the position and velocity weights to 0.15 and ignore the root  $x$  position in the tracking loss.

Finally, the MPPI objective over horizon  $H$  is

$$L_{\text{hop}} = \sum_{t=0}^{H-1} \left( \ell(\mathbf{s}_t, \mathbf{a}_t) + \ell_{\text{ref}}(t) \right). \quad (29)$$

**Accumulated reward.** We report the episode-level accumulated reward using the standard Hopper reward:

$$R_{\text{ep}} = \sum_{t=0}^{T-1} \left( r_{\text{healthy}}(t) + r_{\text{fwd}}(t) - c_{\text{ctrl}}(t) \right). \quad (30)$$

**MPPI parameters.** We use temperature  $\lambda = 0.5$ , horizon  $H = 100$ , and  $N = 256$  sampled trajectories per control cycle.

### D.3.3 Unitree Go1 Robot

**Task.** Following [3], we consider straight walking on flat terrain. The robot tracks a sequence of planar waypoints while following an internal gait reference. Let the Go1 state at time  $t$  be

$$\mathbf{s}_t = [\mathbf{p}_t, \mathbf{q}_t, \mathbf{q}_t^j, \mathbf{v}_t, \boldsymbol{\omega}_t, \dot{\mathbf{q}}_t^j],$$

where  $\mathbf{p}_t \in \mathbb{R}^3$  is the base position,  $\mathbf{q}_t \in \mathbb{H}$  is the base orientation quaternion,  $\mathbf{q}_t^j \in \mathbb{R}^{12}$  are joint angles,  $\mathbf{v}_t \in \mathbb{R}^3$  and  $\boldsymbol{\omega}_t \in \mathbb{R}^3$  are base linear/angular velocities, and  $\dot{\mathbf{q}}_t^j \in \mathbb{R}^{12}$  are joint velocities. The control input  $\mathbf{a}_t \in \mathbb{R}^{12}$  is the commanded joint action.

**Cost for straight walking.** Following [3], we define a tracking objective that penalizes deviations from a desired state reference and a gait-based joint reference:

$$L_{\text{walk}} = \sum_{t=0}^{H-1} \left[ (\mathbf{s}_t^{\text{ref}} - \mathbf{s}_t)^\top \mathbf{Q} (\mathbf{s}_t^{\text{ref}} - \mathbf{s}_t) + (\mathbf{a}_t^{\text{ref}} - \mathbf{a}_t)^\top \mathbf{R} (\mathbf{a}_t^{\text{ref}} - \mathbf{a}_t) \right], \quad (31)$$

where  $\mathbf{s}_t$  and  $\mathbf{a}_t$  denote the robot state and control at time  $t$ , respectively. The state reference  $\mathbf{s}_t^{\text{ref}}$  includes the desired base position and attitude induced by the current waypoint. The control reference  $\mathbf{a}_t^{\text{ref}}$  is given by the gait scheduler [29], and  $\mathbf{Q}$  and  $\mathbf{R}$  are diagonal weight matrices.

**Accumulated reward.** To evaluate performance on the *walk-straight* task, we follow the Gymnasium definition [37] and use the *forward\_reward* for Go1. This reward measures the robot’s planar displacement projected onto the instantaneous direction toward the current goal.

Let an episode be discretized into time steps  $t = 0, 1, \dots, T - 1$ . Denote the robot base position in the world frame as  $\mathbf{p}_t \in \mathbb{R}^3$ , and its planar component as  $p_{t,xy} \in \mathbb{R}^2$ . Let the current goal at time  $t$  be  $g_t \in \mathbb{R}^2$ . For each simulation step, we record the planar position before advancing the dynamics,  $p_{t,xy}^{\text{pre}}$ , and after the dynamics step,  $p_{t,xy}^{\text{post}}$ :

$$p_{t,xy}^{\text{pre}} = p_{t,xy}, \quad p_{t,xy}^{\text{post}} = p_{t+1,xy}. \quad (32)$$

We define the direction to the goal and its normalized form as

$$d_t = g_t - p_{t,xy}^{\text{pre}}, \quad \hat{d}_t = \begin{cases} \frac{d_t}{\|d_t\|_2}, & \|d_t\|_2 \geq \varepsilon, \\ \mathbf{0}, & \text{otherwise,} \end{cases} \quad (33)$$

where  $\varepsilon > 0$  is a small constant used to avoid numerical instability when  $\|d_t\|_2$  is close to zero. Thus,  $\hat{d}_t = \mathbf{0}$  only when the robot is sufficiently close to the goal (i.e.,  $\|d_t\|_2 < \varepsilon$ ); otherwise,  $\hat{d}_t$  is the unit vector pointing from the current position to the goal. (we use  $\varepsilon = 10^{-8}$ ). The planar displacement over one step is

$$\Delta p_t = p_{t,xy}^{\text{post}} - p_{t,xy}^{\text{pre}}. \quad (34)$$

The per-step goal-conditioned forward progress reward is then defined as

$$r_{\text{fwd}}(t) = \Delta p_t^\top \hat{d}_t. \quad (35)$$

Finally, we report the episode-level accumulated forward progress

$$R_{\text{fwd}} = \sum_{t=0}^{T-1} r_{\text{fwd}}(t). \quad (36)$$

**MPPI parameters.** We use temperature  $\lambda = 0.1$ , horizon  $H = 40$ ,  $N = 30$  sampled trajectories per control cycle.

## E Impact of Pretraining on Few-shot Learning

To further quantify the impact of pretraining, we compare few-shot learning curves of WestWorld with and without pretraining. As illustrated in Fig. 6, the pretrained model achieves substantially lower MSE across all 10 fine-tuning episodes on three robots. The performance gap remains large even after convergence, indicating that pretrained WestWorld not only accelerates adaptation but also leads to better final accuracy. These results confirm that our system-aware pretraining enables the model to capture distinct robotic dynamics priors that can be efficiently adapted to new systems with limited data.

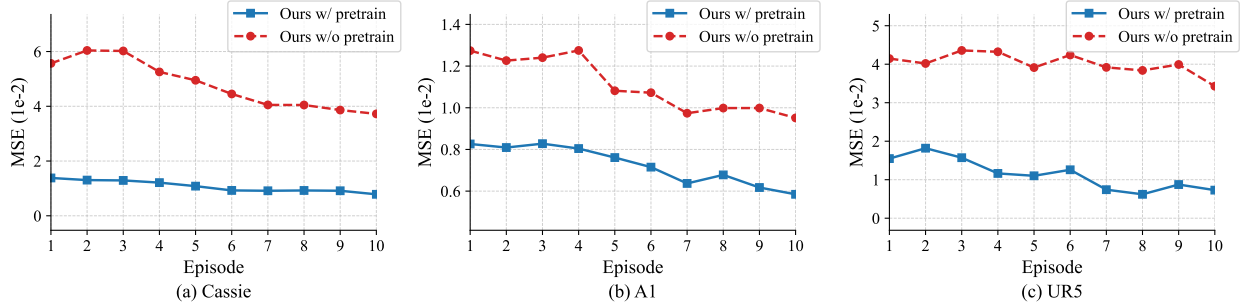


Figure 6: The effect of pre-training on few-shot learning for three different robotic systems: (a) Cassie, (b) A1 and (c) UR5 Robots.

## F Discussion

**Efficient Parameter Finetuning.** When employing the pre-trained model to downstream tasks, fully fine-tuning all model parameters can be memory-intensive. Motivated by parameter-efficient finetuning, we study whether few-shot adaptation can be achieved by updating only a small subset of parameters. In our experiments, we freeze the backbone and fine-tune only (i) the Sys-MoE layers, (ii) the learnable query tokens, and (iii) the final decoder linear head.

Table 11 shows the experimental results by fine-tuning only the last  $j$  Sys-MoE layers ( $j \in \{2, 4, 6\}$ ), and compares them with the full fine-tuning method. It can be seen from this table that the increase of  $j$  can improve prediction performance across Cassie, A1, and UR5 systems. However, fine-tuning only the last few Sys-MoE layers still achieve high accuracy compared to the baseline. Specifically, fine-tuning the last two Sys-MoE layers updates only 21.91% of the parameters, yet it outperforms the fully fine-tuned TrajWorld baseline on all three systems. This result implies that parameter-efficient updates to the Sys-MoE components remain effective even under domain shifts.

Table 11: We compare fine-tuning the last 2/4/6 Sys-MoE layers against full fine-tuning and the best-performing SOTA baseline (TrajWorld). All experiments use a fixed random seed. Lower is better.

Method	Tuned Layers	Tuned Params	MSE ( $\times 10^{-2}$ ) $\downarrow$		
			Cassie	A1	UR5
Trajworld	Full	10.0 M	1.674	0.931	2.616
Ours	Last 2 Sys-MoE	3.2 M (21.91%)	1.249	0.775	1.052
	Last 4 Sys-MoE	6.3 M (43.37%)	1.074	0.762	1.031
	Last 6 Sys-MoE	9.5 M (64.83%)	1.055	0.744	0.895
	Full	14.6 M (100%)	<b>0.785</b>	<b>0.636</b>	<b>0.761</b>

**Computational Cost.** We further compare the inference-time latency of our method with SOTA autoregressive transformer baselines, namely *TDM* [33] and *TrajWorld* [46]. All methods use a fixed-length history window of  $T_{\text{hist}} = 50$  steps as input, with batch size  $B = 4$ , observation dimension  $D_o = 78$ , and action dimension  $D_a = 21$ . We evaluate multi-step prediction horizons  $H \in \{10, 30, 50, 70, 100\}$  on a single NVIDIA RTX A6000 GPU. We report the mean and standard deviation of wall-clock latency (in milliseconds) over 10 repeated runs after warm-up, with CUDA synchronization enabled. For autoregressive baselines, we follow the setup in [46] and use KV-cache decoding to reduce per-step computational overhead. Table 12 summarizes the inference latency for different methods. Our approach consistently achieves fastest inference for long-horizon predictions except for  $H=10$ . This advantage arises from our use of learnable query embeddings, which enable the model to predict all  $H$  future steps in a single forward pass. As a result, our method is approximately  $3.09\times$  faster than *TrajWorld* and  $10.73\times$  faster than *TDM* when  $H = 100$ .

Table 12: Wall-clock latency (ms, mean $\pm$ std) for multi-step prediction on a single NVIDIA RTX A6000. All methods take  $T_{\text{hist}} = 50$  history steps as input ( $B = 4$ ,  $D_o = 78$ ,  $D_a = 21$ ). Results are averaged over 10 repeated runs after warm-up. Lower is better.

Method	Latency (ms) $\downarrow$				
	$H = 10$	$H = 30$	$H = 50$	$H = 70$	$H = 100$
TDM	388.85 $\pm$ 0.41	697.89 $\pm$ 0.64	1099.63 $\pm$ 1.41	1602.34 $\pm$ 1.33	2558.94 $\pm$ 1.64
TrajWorld	<b>94.62<math>\pm</math>0.30</b>	236.63 $\pm$ 0.33	379.43 $\pm$ 0.59	522.37 $\pm$ 0.43	736.67 $\pm$ 0.91
Ours	113.61 $\pm$ 0.71	<b>138.03<math>\pm</math>1.45</b>	<b>159.90<math>\pm</math>0.97</b>	<b>183.96<math>\pm</math>1.01</b>	<b>238.52<math>\pm</math>0.47</b>

## G Real-world Deployment

To enable real-time control on a physical Unitree Go1 at a high control rate (90 Hz), we distill the pretrained WestWorld into a lightweight student model via knowledge distillation (KD) [21], and then fine-tune it using simulation data collected for the downstream control tasks.

**Distillation objective.** We construct a smaller student world model by reducing the backbone depth to two Sys-MoE blocks (with the same discretized prediction head over  $K$  uniform bins as in Eq. (10)). Let  $\mathbf{P}_\ell^{(m)}$  denote the categorical prediction (over  $K$  bins) produced by the pretrained teacher model for channel  $m$  at token index  $\ell$ , and let  $\tilde{\mathbf{P}}_\ell^{(m)}$  be the corresponding student prediction. We train the student with a convex combination of the original next-token cross-entropy loss and a soft distillation loss:

$$\mathcal{L}_{\text{KD}} = \alpha \mathcal{L}_{\text{CE}} + (1 - \alpha) \mathcal{L}_{\text{soft}}, \quad (37)$$

where  $\mathcal{L}_{\text{CE}}$  is the same next-token loss in Eq. (11), and the soft loss matches the student distribution to the teacher distribution:

$$\mathcal{L}_{\text{soft}} = - \sum_{\ell=1}^{L-1} \sum_{m=1}^{M_s} \mathbf{P}_\ell^{(m)\top} \log \tilde{\mathbf{P}}_\ell^{(m)}. \quad (38)$$

We set  $\alpha = 0.9$  in the KD experiments.

**Distillation and fine-tuning settings.** We first distill the student model on the same pretraining trajectories by using the teacher outputs  $\mathbf{P}_\ell^{(m)}$  as soft targets, while keeping the ground-truth token supervision through  $\mathcal{L}_{\text{CE}}$ . After distillation, we fine-tune the student on the simulation dataset collected for downstream control (Section C.5), following the same optimizer and early-stopping protocol as in the downstream control training settings (Section D.2).